

Modelling electroweak physics for the forward region

M. Sirendi^{1,2}

¹*Cavendish Laboratory, University of Cambridge, United Kingdom*

²*Dept. of Astronomy and Theoretical Physics, Lund University, Sweden*

Abstract

This note presents a study of matching and merging schemes and weak showering at the LHC as applied to the production of electroweak bosons in association with jets. These advanced theoretical tools are seen to provide a good description of event shapes in the central region when compared to measurements performed by the ATLAS and CMS collaborations at a centre-of-mass energy of 7 TeV. Matching and merging schemes also provide a superior description of forward Z +jets production. The study constitutes a test of matching and merging schemes in a novel region of phase space and can be considered as a validation of the universality of these techniques. Finally, it was determined that current measurements of electroweak physics at LHCb do not yet fully probe the effect of weak showers.

Contents

1	Introduction	1
2	The hadroproduction of weak gauge bosons	2
3	The parton shower framework	4
4	Matching matrix elements to parton showers	6
4.1	The MLM scheme	9
4.2	Unitarised matrix element + parton shower merging	9
4.3	The FxFx scheme	9
4.4	Merging NLO matrix elements with parton showers	9
4.5	The appropriate choice of PDF	10
5	Results on matching and merging	10
6	Weak gauge boson emission in parton showers	14
7	Results on weak showering	14
8	Conclusions	22
9	Acknowledgements	22
	References	23

1 Introduction

The study of Z/W +jets production¹ in pp collisions serves as a testing ground for theoretical predictions derived from perturbative quantum chromodynamics (pQCD) and electroweak (EW) theory. These processes are also a ubiquitous background to physics beyond the Standard Model (SM) and so must be precisely measured and theoretically understood. Measurements performed by the ATLAS [1–3], CMS [4–6], and LHCb [7–14] collaborations are in good agreement with theoretical predictions that are determined from parton-parton cross-sections convolved with parton distribution functions (PDFs). The precision of these predictions is limited by the accuracy of the PDFs and by higher-order QCD corrections which are currently known at next-to-next-to-leading order (NNLO) in pQCD [15, 16].

Two conventional theoretical tools employed in high energy physics to make QCD predictions are fixed order calculations and Monte Carlo (MC) event generators. Fixed order calculations are limited in their ability to describe event topologies with many jets. Conversely, MC event generators commonly employ the parton shower (PS) formalism which approximates parton emissions to all orders and multiplicities. This approach, however, mismodels the number, and hardness, of jets due to its approximate nature.

This note concerns itself with the study of two novel theoretical approaches for rectifying the above issues: matching and merging (M&M) and weak showering (WS). M&M seeks to unite a matrix element (ME) calculation at a given order in pQCD with the PS. On the other hand, WS improves the PS description of jet formation by allowing for the emission of EW bosons within the jet. In particular, this note will compare these theoretical approaches to measurements performed by the LHCb experiment in the forward region at the LHC. The LHCb detector, which is instrumented in the pseudorapidity range $2.0 < \eta < 5.0$, is in a unique situation to validate the universality of these techniques and act as a complementary test to measurements performed by the ATLAS and CMS collaborations.

There are several other theoretical effects that affect the performance of these predictions such as higher order quantum electrodynamic (QED) and EW corrections, their interplay and effect on pQCD corrections. Within the realm of MC event generators, the tuning of the PS and multiparton interactions (MPI) becomes important. Finally, uncertainties due to PDFs enter and can become particularly large at high and low values of Bjorken- x which corresponds to the kinematic acceptance of the LHCb detector. While this note seeks to contrast different M&M schemes and test the WS formalism, other studies have devoted considerable effort in understanding the other effects mentioned [17, 18].

In this note, we present an overview of fixed order calculations and the factorisation theorem in Sect. 2, an introduction to the PS formalism in Sect. 3, a comparison of M&M schemes in Sect. 4 and an explanation of WS in Sect. 6. We compare M&M schemes and WS to measurements performed by ATLAS [19], CMS [20, 21], and LHCb [22] at a centre-of-mass energy of $\sqrt{s} = 7$ TeV. We also compare M&M schemes to a measurement of inclusive Z production by LHCb at $\sqrt{s} = 13$ TeV [14].

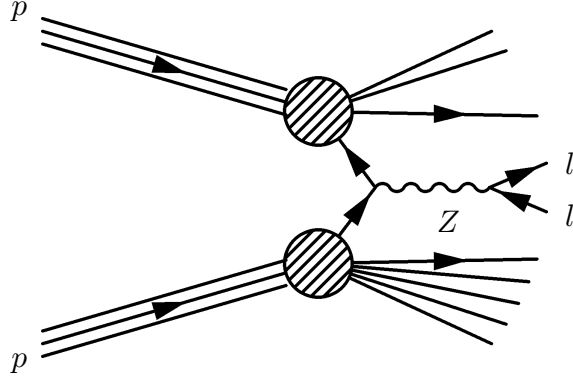


Figure 1: The Drell-Yan process for producing a Z boson in a pp collision.

2 The hadroproduction of weak gauge bosons

Drell and Yan first proposed that a scattering cross-section in hadronic collisions can be treated as a convolution of the partonic cross-section, calculable in pQCD, and the distributions of parton momentum in the proton, given by a PDF [23]. The archetypal example for the procedure is provided by the Drell-Yan interaction, illustrated in Fig. 1. However, it has been successfully extended to other processes and, crucially, it enables higher order QCD corrections to be incorporated. In general, a cross-section, $\sigma_{pp \rightarrow X}$, summed over initial state partons a and b with momentum fractions x_a and x_b , with PDFs $f_a(x_a)$ and $f_b(x_b)$, and at a given energy scale Q is

$$\sigma_{pp \rightarrow X} = \text{PDF} \otimes \hat{\sigma}_{ab \rightarrow X} = \sum_{a,b} \int dx_a dx_b f_a(x_a, Q^2) f_b(x_b, Q^2) \hat{\sigma}_{ab \rightarrow X}(Q^2). \quad (1)$$

The partonic cross-section, $\hat{\sigma}_{ab \rightarrow X}$, is calculated as a power series expansion in the strong coupling constant, α_s , with further terms corresponding to higher order emissions:

$$\hat{\sigma}_{ab \rightarrow X} = [\hat{\sigma}_{\text{LO}} + \alpha_s \hat{\sigma}_{\text{NLO}} + \alpha_s^2 \hat{\sigma}_{\text{NNLO}} + \dots]_{ab \rightarrow X}. \quad (2)$$

Feynman diagrams for leading virtual and real corrections (*i.e.* NLO) are illustrated in Fig. 2. The higher order terms increase the LO cross-section for W and Z bosons by about 20 – 30% [24] and are needed to reproduce the boson transverse momentum, $p_T^{Z/W}$, spectrum observed in data. Generally, the precision of the measurement dictates the order of the perturbative calculation that must be performed to make a valid comparison.

For the Drell-Yan process specifically terms up to $\mathcal{O}(\alpha_s^2)$ have been computed [25] with recent progress on the N³LO calculation [26]. However, as the number of Feynman diagrams increases roughly factorially with each order in perturbation theory, it becomes increasingly difficult to extend the precision of these calculations. What is more, at this order in α_s QED and EW corrections become comparable in size and must also be computed.

There is also an additional difficulty with this approach. Namely, when the mass of the boson, $M_{Z/W}$, is significantly greater than its $p_T^{Z/W}$ (*i.e.* close to threshold production), higher-order terms become large and spoil the convergence of the series. In particular, the

¹Throughout this note Z denotes the combined Z and virtual photon (γ^*) contribution.

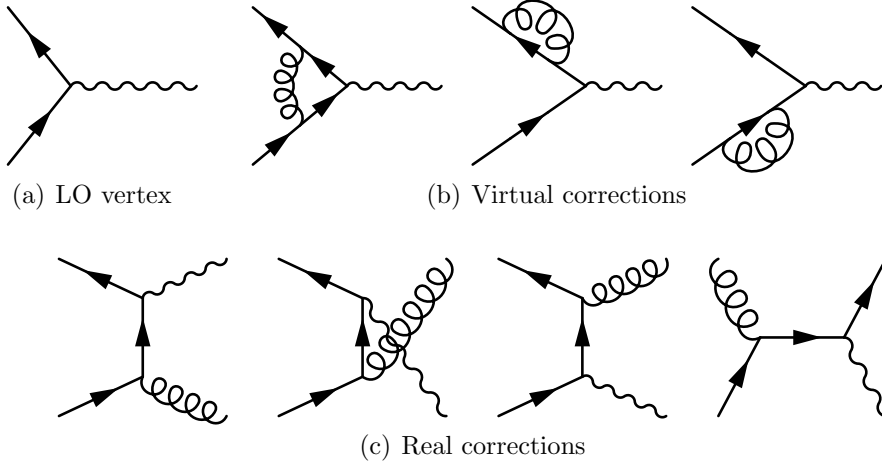


Figure 2: The LO interaction vertex with first order corrections.

emission of multiple soft gluons must be considered. The leading contributions at each order are proportional to

$$\alpha_s \ln \frac{M_{Z/W}^2}{(p_T^{Z/W})^2}. \quad (3)$$

Clearly these logarithms are significant when $p_T^{Z/W}$ is small. In fact, after taking prefactors into account, these terms become $\mathcal{O}(1)$ for $p_T^{Z/W}$ values² less than 10 – 15 GeV [24]. Fortunately, these terms can be resummed to all orders. This is particularly advantageous near the boundaries of phase space where fixed order calculations break down. The method of resumming logarithms has been implemented in the RESBOS [27–29] event generator where next-to-next-to-leading log (NNLL) corrections are computed for NLO differential cross-sections.

The inclusive Z or W cross-section can also be decomposed into its multijet components, formulated as

$$\sigma_{Z/W} = \sigma_{Z/W+0\text{jets}} + \sigma_{Z/W+1\text{jets}} + \sigma_{Z/W+2\text{jets}} + \sigma_{Z/W+n\text{jets}} + \dots, \quad (4)$$

where n is the number of jets and also sets the lowest power of α_s in the expansion of each term. In this study cross-sections for $\sigma_{Z/W+0\text{jets}}$ and $\sigma_{Z/W+1\text{jets}}$ are computed to NLO, while LO MEs are used for $\sigma_{Z/W+2\text{jets}}$. Provided the jets are energetic and well-separated, this serves as a reasonable approximation to the multijet cross-section. However, a PS is needed to extend the jet multiplicity beyond that, to describe collinear and infrared emissions, and to provide a natural entry point into hadronisation models. The basics of the PS formalism will now be outlined.

²Natural units with $\hbar = c = 1$ are used throughout.

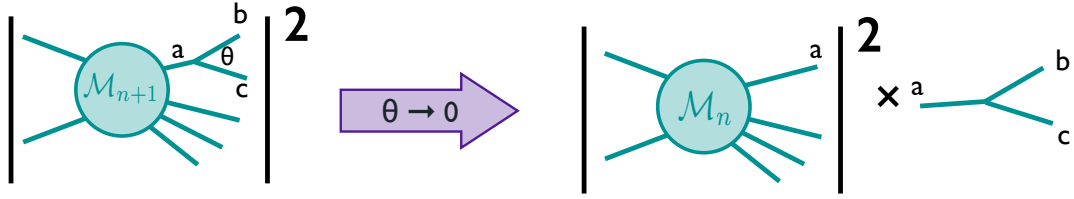


Figure 3: The production of $n + 1$ outgoing particles can be described as the product of the n -particle ME and the $a \rightarrow bc$ branching provided $\theta \rightarrow 0$. Figure taken from [30].

3 The parton shower framework

While the previous section discusses the issues involved with performing a precise pQCD calculation at fixed order in perturbation theory, this section presents an alternative approach where an approximate calculation is carried out to all orders in α_s . A calculation that encompasses higher orders is particularly relevant for collinear branchings and the emission of soft partons. Splittings of the type $q \rightarrow qg$, $\bar{q} \rightarrow \bar{q}g$, $g \rightarrow q\bar{q}$ will be considered, all with QED counterparts, along with the $g \rightarrow gg$ branching which stems from the non-Abelian nature of QCD³. The tree-level MEs for these branchings are divergent unless virtual corrections are computed, with the exception of $g \rightarrow q\bar{q}$ which does not have an infrared divergence (but does still have a collinear divergence).

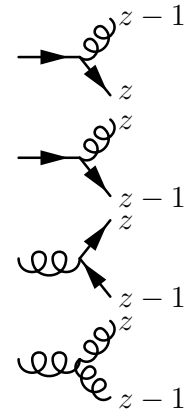
To begin, consider a hard scattering interaction that leads to $n + 1$ outgoing partons. Suppose that within this process particle a branches to b and c at an angle θ . Letting $\theta \rightarrow 0$, a becomes nearly on-shell with a time scale for the branching that is considerably longer than the one characteristic of the hard subprocess. In this limit, the interaction can be described as a product of the ME for the production of n particles and the $a \rightarrow bc$ branching as illustrated in Fig. 3. Formally, the collinear factorisation of the interaction can be expressed as

$$|\mathcal{M}_{n+1}|^2 d\Phi_{n+1} \approx |\mathcal{M}_n|^2 \Phi_n \frac{dt}{t} dz \frac{d\xi}{2\pi} \frac{\alpha_s}{2\pi} P_{a \rightarrow bc}(z), \quad (5)$$

where \mathcal{M} is a ME, Φ denotes phase space, and other terms are explained in what follows.

The branchings are characterised by the energy fraction $z = E_b/E_a$ carried by one of the emerging partons, and an ordering (or evolution) variable t such that each subsequent emission has decreasing t . There is some freedom in the choice of the physical form of t . One possibility is to use the virtuality of the mother parton while other common choices include transverse momentum and the energy-weighted opening angle of emission. Here, ξ is the angle between the polarisation of a and the plane of the branching. The functions $P_{a \rightarrow bc}(z)$ are known as the Dokshitzer-Gribov-Lipatov-Altarelli-Parisi [31–33] splitting kernels. The spin-averaged kernels are

³While the formalism outlined in this section deals with QCD emissions, it should be emphasised that QED emissions can be handled in a similar manner.

$$\begin{aligned}
\hat{P}_{q \rightarrow qg}(z) &= C_F \left[\frac{1+z^2}{1-z} \right], \\
\hat{P}_{q \rightarrow gq}(z) &= C_F \left[\frac{1+(1-z)^2}{z} \right], \\
\hat{P}_{g \rightarrow qq}(z) &= T_R [z^2 + (1-z)^2], \\
\hat{P}_{g \rightarrow gg}(z) &= C_A \left[\frac{z}{1-z} + \frac{1-z}{z} + z(1-z) \right],
\end{aligned}
\tag{6}$$


where $C_F = \frac{4}{3}$, $C_A = 3$, and $T_R = \frac{1}{2}$. Eqs. 6 illustrate that gluons radiate the most, and that the $g \rightarrow qq$ splitting does not have a soft divergence.

Proceeding by considering \mathcal{M}_{n+1} as the core process with an additional $b \rightarrow de$ branching, the differential cross-section becomes

$$\begin{aligned}
|\mathcal{M}_{n+2}|^2 d\Phi_{n+2} &\approx |\mathcal{M}_n|^2 \Phi_n \frac{dt}{t} dz \frac{d\xi}{2\pi} \frac{\alpha_s}{2\pi} P_{a \rightarrow bc}(z) \\
&\times \frac{dt'}{t'} dz' \frac{d\xi'}{2\pi} \frac{\alpha_s}{2\pi} P_{b \rightarrow de}(z').
\end{aligned}
\tag{7}$$

This procedure can be extended to an arbitrary number of emissions, each with an independent branching probability.

Having established the machinery for real emissions, virtual corrections and non-resolvable emissions (as in Fig. 4) must also be accounted for such that unitarity is ensured and divergences are counterbalanced. This is achieved by computing a non-emission probability, known as a Sudakov form factor, that is conventionally labelled as Δ . The differential probability, \mathcal{P} , for a branching to not occur at scale t is

$$d\mathcal{P}_{non-emission}(t) = 1 - d\mathcal{P}_{emission}(t) = 1 - \frac{dt}{t} \frac{\alpha_s}{2\pi} \int dz \hat{P}(z).
\tag{8}$$

Therefore, the probability for no branchings to occur between scales t_1 and t_2 split into N infinitesimal subranges, *i.e.* the Sudakov form factor, is

$$\begin{aligned}
\Delta(t_1, t_2) &= \lim_{N \rightarrow \infty} \prod_{i=0}^N \left(1 - \frac{dt}{t_i} \frac{\alpha_s}{2\pi} \int dz \hat{P}(z) \right), \\
&\simeq \lim_{N \rightarrow \infty} \exp \left(\sum_{i=0}^N \left(-\frac{dt}{t_i} \frac{\alpha_s}{2\pi} \int dz \hat{P}(z) \right) \right), \\
&\simeq \exp \left(-\frac{\alpha_s}{2\pi} \int_{t_1}^{t_2} \frac{dt}{t} \int dz \hat{P}(z) \right).
\end{aligned}
\tag{9}$$

With the emission and non-emission probabilities specified, the cascade of partons can be evolved down to a certain virtuality, conventionally $\mathcal{O}(1 \text{ GeV})$, and a hadronisation model is then applied. A MC event generator implements this model for final-state



Figure 4: Virtual corrections and unresolvable emissions are accounted for via a Sudakov form factor which gives the probability for no branching to occur between two points along the PS evolution.

showers as a Markov chain *i.e.* with independent randomly generated splittings. Initial-state showers are treated in a similar fashion working backwards from the hard interaction to earlier branchings with the added complication that a PDF weight must be applied to each branching.

The PS framework thus offers a robust, physical way of treating multiple splittings to an arbitrary number of partons. The formalism can be applied to generate a timelike shower to describe jets in the final state or evolved backward from the hard interaction to model initial-state radiation. Crucially, it can be shown that the effect of a PS is unitary *i.e.* it leaves the inclusive cross-section unchanged [34]. The PS also gives an approximate estimate of the effect of higher order corrections that can become large at edges of phase space. In addition, it is a natural gateway to the non-perturbative regime of QCD where hadronisation models are employed. Finally, the method is well suited for computer implementation and forms the basis for several MC event generators.

As the PS approximation is strictly true only in the collinear limit and does not fully account for quantum interference, input from a precise ME calculation is typically needed to improve the description of well-separated jets and measures of event shape. This marriage of a ME calculation to a PS is the focus of the next section.

4 Matching matrix elements to parton showers

As the previous sections illuminate, ME and PS calculations have different virtues and ranges of applicability. The strengths and weaknesses of both approaches are summarised in Table 1. Ultimately, it is desirable to accurately describe both the hard process and the development of partons into jets. This achieved by interfacing a ME calculation and a PS. The combination would use a $Z/W + (0, 1, \dots, n)$ parton ME for events with up to n hard jets and dress up the outgoing partons with radiation using the PS. Given that n is finite, additional jets must then arise from PS emissions. In this manner, a more accurate description of events with up to n jets is achieved and the precision of the inclusive cross-section is improved.

Specifically, a given $(m+1)$ -jet event, where $0 \leq m < n$, can be obtained in two ways: from the PS evolution of a $(m+1)$ -parton ME without branchings hard enough to produce a jet; or from a m -parton ME, where the PS leads to the formation of an additional jet. A particular M&M scheme defines which of the two paths should be followed on an event-by-event basis.

The potential pitfalls with this approach are double counting and the biased filling of phase space. Double counting arises when an identical final state is allowed to be generated by both a $(m+1)$ -parton ME and a m -parton ME with an extra jet from the

Matrix element	Parton shower
Good description of well-separated hard partons	Resums to all orders
Exact to given order in perturbation theory	Arbitrary particle multiplicity \Rightarrow ideal for description of jet formation
Quantum interference correct	Hadronisation model easily applied
Limited number of particles	Computationally cheap
Computationally expensive	Valid in collinear limit
Hadronisation model difficult to implement	Quantum interference not fully accounted for

Table 1: Pros and cons of ME and PS descriptions of jet formation.

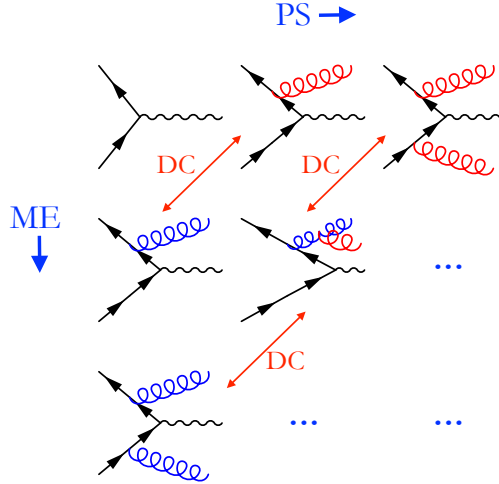


Figure 5: Branchings in the PS (in red) and real emissions in a ME calculation (in blue) can lead one to double count (DC) configurations with the same number of outgoing particles.

PS. This is illustrated for increasing multiplicities in Fig. 5. The solution is to introduce a phase-space separation, referred to as a matching scale, that vetoes PS emissions above a certain threshold. In other words, the PS is only allowed to generate unresolved emissions for multiplicities for which there is a ME calculation available.

In this study, the ME-based sample was required to have jets with transverse momentum, p_T^{jet} , in excess of 10 GeV, where the jets are clustered using the longitudinally-invariant k_T -clustering algorithm for hadron-hadron collisions [35]. The k_T -scheme defines two final-state particles i and j as belonging to separate jets if their relative transverse momentum squared,

$$k_{Tij}^2 = 2 \min(p_{Ti}, p_{Tj})^2 \frac{(\cosh(\eta_i - \eta_j) - \cos(\phi_i - \phi_j))}{R^2}, \quad (10)$$

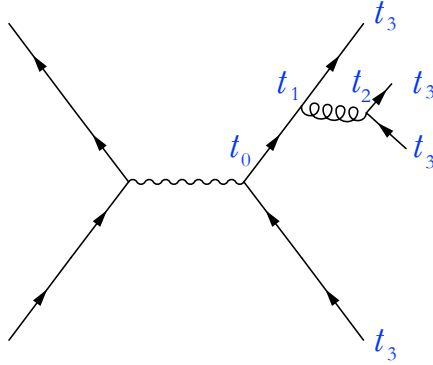


Figure 6: A $2 \rightarrow 4$ process with gluon emission and subsequent splitting to illustrate the relevant scales for α_s reweighting and Sudakov suppression of the ME.

is larger than $(10 \text{ GeV})^2$, where R is a parameter that controls the size of the jet, η is the pseudorapidity and ϕ is the azimuthal angle. The threshold effectively controls the relative weights given to the ME calculation and the PS. A low threshold enhances the contribution from the ME while a high scale gives a bigger role to the shower approximation.

One must also make sure that there is a smooth transition along the phase space boundary between the ME calculation and the PS. This is achieved by two modifications to the ME. Firstly, the ME must be reweighted for the value of α_s that would have been used had the configuration been generated by a PS, which uses a running value of α_s . Secondly, the PS employs Sudakov factors for the non-emission probability. This requires a pseudo-PS history to be created for each ME-based event and a Sudakov reweighting applied to it. This history interprets a particular final state as the result of a sequence of branchings in a PS. Clearly, there is no unique history for a given event so all histories must be generated and one chosen probabilistically. For the configuration shown in Fig. 6 with a starting scale of t_0 and emissions at t_1 and t_2 , the ME becomes

$$|\mathcal{M}|^2 \rightarrow |\mathcal{M}|^2 \frac{\alpha_s(t_1)}{\alpha_s(t_0)} \frac{\alpha_s(t_2)}{\alpha_s(t_0)} (\Delta_q(t_3, t_0))^2 \Delta_g(t_2, t_1) (\Delta_q(t_3, t_2))^2, \quad (11)$$

where t_3 is the endpoint of the evolution in this example. Sudakov suppression also serves to make MEs exclusive such that different parton multiplicities can be added *i.e.* merged.

Several prescriptions have been proposed to resolve the issues of avoiding double counting and ensuring a smooth transition between hard and soft regimes. Additionally, these approaches differ in their treatment of higher orders in the ME calculation. One strategy is to extend real emissions to higher orders at LO accuracy while approximating virtual/loop corrections with shower Sudakov factors. Alternatively, NLO MEs can be used for the first few emissions. The CKKW [36], CKKW-L [37–40], MLM [41], and UMEPS [34] schemes employ LO MEs while NLO MEs are used in FxFx [42] and UNLOPS [43]. Finally, NNLO MEs have been employed for Drell-Yan and Higgs physics in the UN²LOPS scheme [44, 45].

What follows is an overview of the different M&M schemes that were included in this study with emphasis on the differences between them.

4.1 The MLM scheme

Two earlier M&M schemes, CKKW and CKKW-L, examine individual branchings within a PS and reject those with $t_i > t_{\text{MS}}$ for branching i and matching scale t_{MS} to establish a phase space division. However, this form of truncated showering requires a modification of the showering algorithm. The innovation of the MLM scheme is to evolve the PS from t_0 to the hadronisation scale, form jets and reject the event if a shower-initiated jet exceeds the matching scale. The scheme is attractively simple by enabling matching to any shower algorithm without requiring modifications. However, the Sudakov suppression of the ME is, as a consequence, imprecise since a product of Sudakov factors that the jet represents is substituted for the factor associated to a single branching.

4.2 Unitarised matrix element + parton shower merging

As previously mentioned, it can be shown that the PS does not modify the total cross-section - a property known as PS unitarity. However, since there is only a partial correspondence between m -jet MEs and an equivalent sequence of approximate splitting kernels, the total cross-section is modified in the CKKW-L M&M scheme. Specifically, the PS is generally correct to LL or NLL accuracy. Therefore, a residual mismatch remains for further subleading terms.

UMEPS resolves this mismatch by explicitly integrating over the phase space of a jet in the m -jet sample to arrive at a virtual correction to the $(m - 1)$ -jet sample. This enables the scheme to better describe unresolvable emissions at any multiplicity and enforces a cancellation between real and virtual terms for any multiplicity. In this manner the unitarity of the inclusive cross section is enforced. The cancellation of unresolved and resolved contributions also significantly reduces the scheme's dependence on the choice of matching scale.

4.3 The FxFx scheme

If all jets in a process are the result of PS emissions, one obtains an inclusive cross-section which is LO+LL accurate with LL accurate exclusive observables⁴. The purpose of tree-level M&M schemes is to improve the description of exclusive observables with LO MEs. The aim of the FxFx scheme is to promote exclusive observables to NLO+LL accuracy. This is advantageous as the precision of collider phenomenology is improved and scale uncertainties are greatly reduced. In the FxFx scheme, the m -parton cross-section is calculated using the MC@NLO procedure [46] and the matching to the PS is handled according to the MLM procedure. Unlike other schemes, the matching scale can be replaced by a smooth monotonic function (effectively, a matching range).

4.4 Merging NLO matrix elements with parton showers

Multi-jet tree-level merging improves event shapes but cannot give a correct overall normalisation or decrease the uncertainty deriving from scale variations. The UNLOPS

⁴If the definition of a given observable explicitly involves m jets, it is considered exclusive in m jets and inclusive in $n - m$ jets with $0 \leq m \leq n$. When $m = 0$, the observable is typically called fully inclusive.

method aims to have a NLO accurate description of exclusive m -jet final states while also ensuring the unitarity of the overall cross-section in a manner inspired by the UMEPS scheme. In this spirit, once a one-jet NLO calculation is added, its integrated version is used to correct zero-jet events and similarly for all multiplicities that MEs are available for. The precision of the method is further improved by including tree-level MEs for multiplicities beyond those for which an NLO calculation is available. These multiplicities are handled in a manner similar to that of UMEPS. Analogously to UMEPS, variations caused by a dependence on the matching scale are minimised due to the “subtract what you add” principle. Finally, it is also worth pointing out that the scheme can be straightforwardly promoted to NNLO accuracy (termed UN²LOPS) as is established in Refs. [44, 45].

4.5 The appropriate choice of PDF

A NLO ME calculation gives an enhancement of a factor $\ln(1/x)$ that is compensated by a commensurate term in a NLO PDF. It is crucial that the order of the ME and the PDF match, particularly for small x where $\ln(1/x)$ is large. Therefore, a LO PDF is used for the PS and MPI.

5 Results on matching and merging

This study is carried out using PYTHIA 8.201 [47]. Events based on MEs are generated externally using the aMC@NLO framework as implemented in MADGRAPH 5.2.3.2.2 [48] and interfaced to PYTHIA using LHE-files [49]. The NLO M&M schemes have a NLO CT10 PDF set [50] in the ME-level calculation, while the LO CTEQ6L1 PDF set [51] is employed for LO M&M schemes. The CTEQ6L1 PDF set is also used for the PS and for MPI within PYTHIA. α_s is set to 0.118 at the Z mass in the ME calculation and a value of 0.1365 is used for modelling the remainder of the event. The matching scale is set at 10 GeV. All comparisons to LHC measurements are carried out within the RIVET framework [52].

The standard LO description of weak gauge boson production is referred to as the “Born description” in what follows. MLM is LO up to 2 jets; FxFx is NLO to 1 jets; UNLOPS is NLO to 1 jets and LO up to 2 jets. Higher jet multiplicities are generated by the PS. In the central region the predictions are compared to measurements by ATLAS [19] and CMS [20] at $\sqrt{s} = 7$ TeV. At the same centre-of-mass energy, a LHCb measurement of Z +jets [22] is used to gauge agreement in the forward region. Finally, the predictions are compared to a measurement of inclusive Z production in the forward region at $\sqrt{s} = 13$ TeV [14].

Fig. 7 illustrates that M&M schemes clearly outperform the Born description in modelling event shapes such as the angle between jets or between the Z boson and the jets. No significant differences between the M&M schemes are observed.

Figs. 8 and 9 (a) illustrate that certain regions of phase space are poorly modelled in the forward region by the Born description. Discrepancies are seen in the first bin of Fig. 8 (a), which corresponds to events with multiple hard jets, but low Z boson p_T , p_T^Z . Also, the slope of the differential cross-section as a function of p_T^{jet} is incorrect. Due to momentum conservation, mismodelling of p_T^{jet} also has an impact on p_T^Z and, by extension,

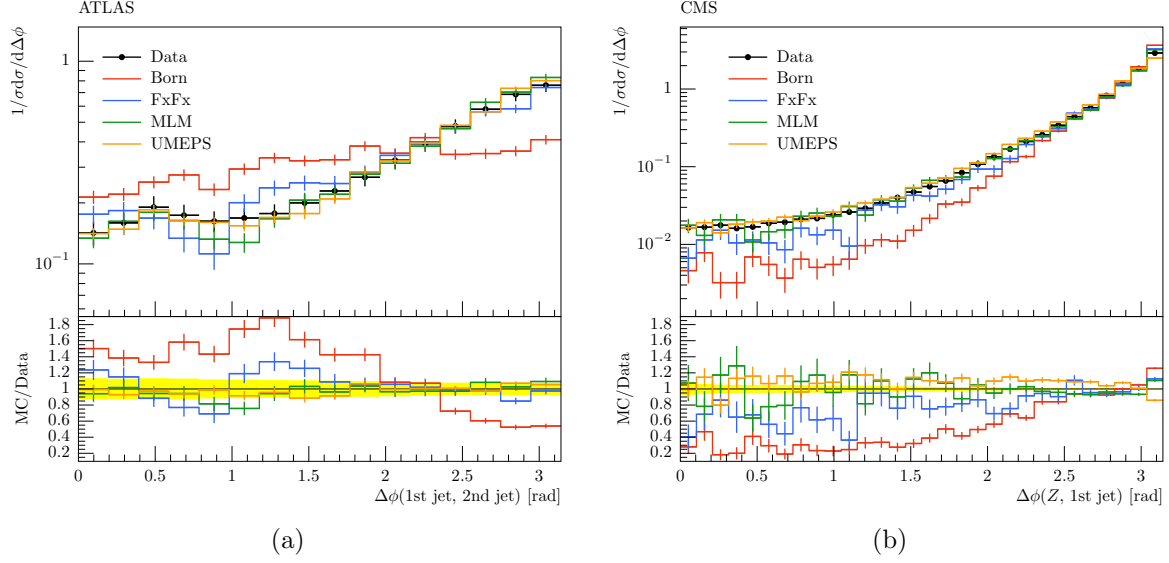


Figure 7: The normalised differential cross-section for Z +jets production in leptonic final states as a function of the (a) azimuthal angle between the leading and subleading jet and (b) the Z boson and the leading jet as measured by (a) ATLAS [19] and (b) CMS [20]. Data points with full uncertainties are compared to the Born description in red and a selection of M&M schemes. Simulation uncertainties are statistical only.

the p_T of the daughter leptons. Finally, the Born description predicts a larger number of pencil-like event topologies when compared to the measurement and to the predictions from M&M schemes as seen in Fig. 9 (a). Fig. 9 (b) gives the difference in rapidity between the Z boson and the leading jet with no significant differences seen between the predictions. Overall, it is clear that M&M schemes offer a superior description of event topologies with multiple hard jets in the forward region.

Fig. 10 illustrates that M&M schemes model the ϕ_η^* distribution⁵ and p_T^Z well. UNLOPS is slightly discrepant due to the lack of a dedicated tune for NLO M&M methods in PYTHIA. Finally, it is worth noting that none of the M&M schemes have the correct overall cross-section in the forward region with discrepancies at the 5% level. This suggests corrections beyond NLO are crucial and UN²LOPS should ideally be used.

⁵Relying solely on angles, ϕ_η^* acts as a proxy for transverse momentum. It is defined as $\phi_\eta^* \equiv \tan \frac{\pi - |\Delta\phi|}{2} / \cosh \frac{\Delta\eta}{2} \simeq p_T/M$, where M and p_T refer to the lepton pair, $\Delta\eta$ and $\Delta\phi$ are the differences in pseudorapidity and azimuthal angles respectively between the leptons.

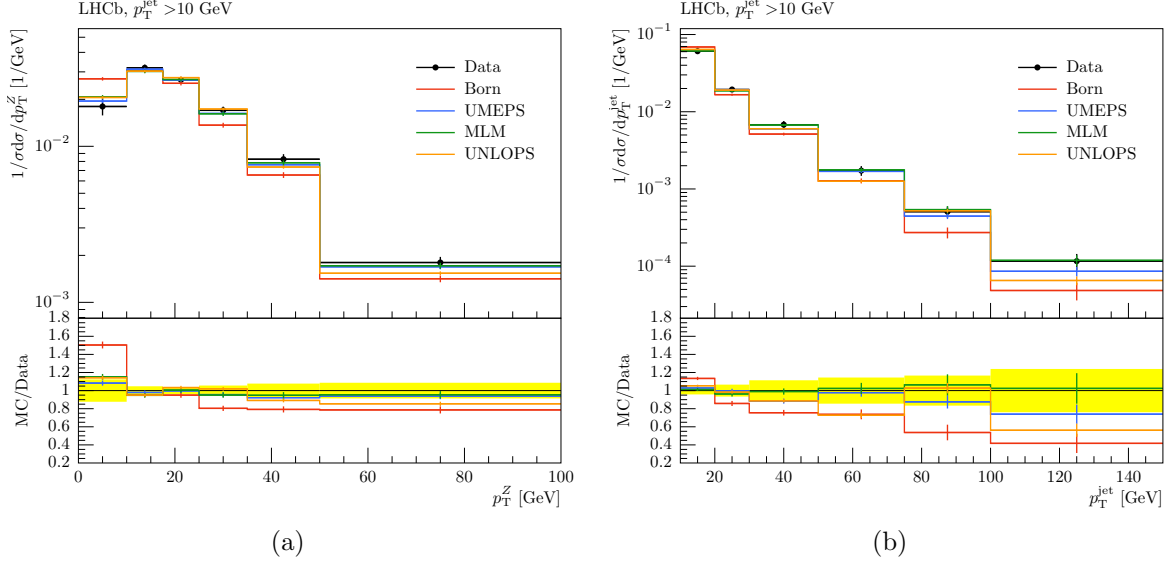


Figure 8: The normalised differential cross-section for Z +jets production in the muon final state as a function of the (a) transverse momentum of the Z and (b) the transverse momentum of the leading jet as measured by LHCb [22]. Data points with full uncertainties are compared to the Born description in red and a selection of M&M schemes. Simulation uncertainties are statistical only.

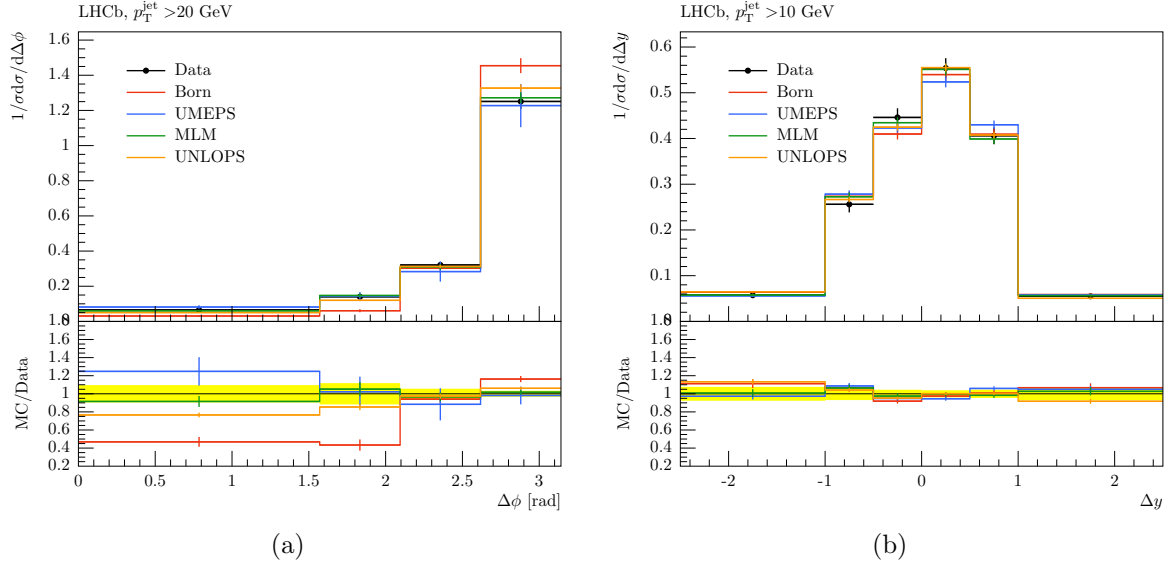


Figure 9: The normalised differential cross-section for Z +jets production in the muon final state as a function of the (a) azimuthal angle and (b) the rapidity between the Z boson and the leading jet as measured by LHCb [22]. Data points with full uncertainties are compared to the Born description in red and a selection of M&M schemes. Simulation uncertainties are statistical only.

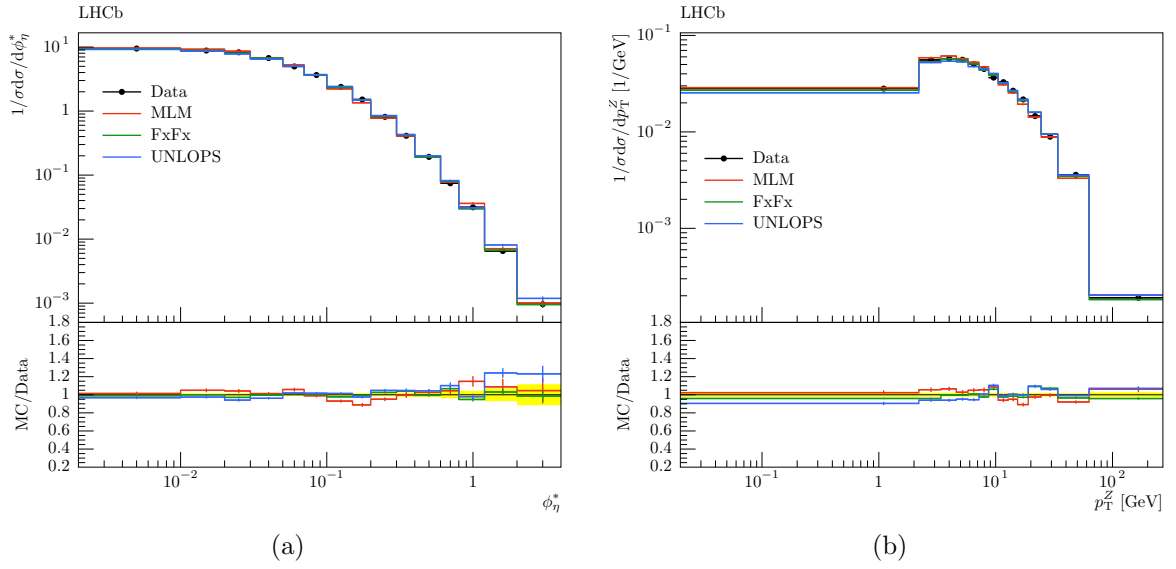


Figure 10: The normalised differential cross-section for inclusive Z boson production in the muon final state as a function of (a) ϕ_η^* and (b) the transverse momentum of the Z as measured by LHCb [14]. Data points with full uncertainties are compared to a selection of M&M schemes. Simulation uncertainties are statistical only.

6 Weak gauge boson emission in parton showers

WS approaches Z and W production from a novel viewpoint. In a Born description of weak gauge boson production the hardest scale in the event is associated with creating the bosons and any jet activity is modelled by means of a PS originating from initial- or final-state radiation, and MPI. This, however, will typically underestimate the number, and hardness, of associated jets. WS instead starts from a QCD process, most commonly dijet production, and allows for the emission of Z and W bosons within the development of the PS [53]. For this purpose, appropriate splitting kernels must be implemented and the helicity of the weak boson daughters accounted for. An additional complication is the relatively high mass of EW bosons which leads to kinematic constraints. In PYTHIA, energy-momentum conservation is achieved by treating MPI, initial- and final-state radiation together such that all features of the event are in direct competition for phase space [54].

The Born description and WS can be added to populate the phase space more fully and to achieve a better description of EW physics in an hadronic environment with centre-of-mass energies that can greatly exceed the EW scale. While these two production paths are expected to preferentially populate different regions of phase space, it is clear that their combination can result in double counting. Since both production modes can lead to topologies with the same number of final state jets, care must be taken to veto events which are better described by the competing production path. This is achieved by employing the k_T -clustering algorithm on all final-state particles, including weak bosons. Events with bosons lying close to jets in a Born description and, correspondingly, events with bosons that are separated from jets in the QCD-initiated path are vetoed.

Extending the PS machinery to include EW boson emissions brings several improvements to the simulation of high-energy pp collisions. Experimentally, weak bosons are seen to be present in jets from their leptonic signatures and the emission probability increases as a function of the centre-of-mass energy of the collision. Weak emission, therefore, can lead to a more realistic description of jet substructure which complements the many ongoing experimental efforts to study the internal structure of jets and formulate discriminating variables based on this [55].

Secondly, weak corrections are required to reproduce the jet rate suppression expected at p_T^{jet} values in excess of 1 TeV. What is more, the WS machinery complements efforts in developing M&M schemes. As explained previously, M&M schemes require PS histories to be generated for Sudakov suppression terms. Allowing for EW emission in the PS leads to more realistic histories and also enables histories to be generated for processes which currently lack one.

Finally, this study seeks to test if a better description of EW boson production in association with jets can be achieved with WS. In particular, WS is expected to be relevant for events with hard jets and high jet multiplicities.

7 Results on weak showering

In this section the Born description of Z or W production and simulation of dijet production along with weak emissions within the PS are compared to measurements made at ATLAS [19], CMS [21], and LHCb [22] at $\sqrt{s} = 7$ TeV. PDFs are parameterised by

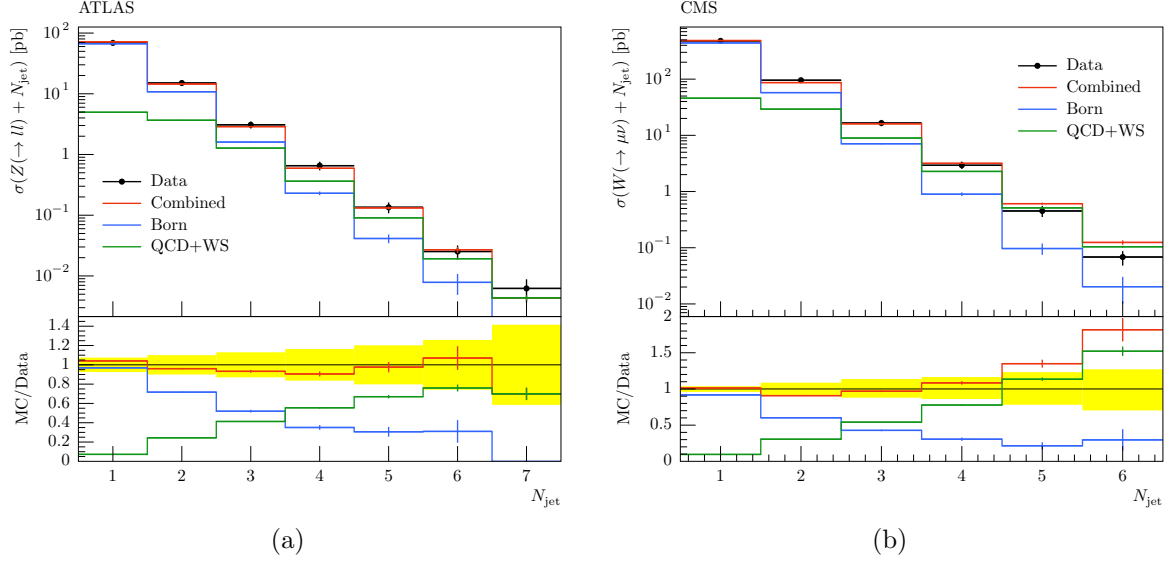


Figure 11: Differential cross-section for (a) Z +jets production and (b) W +jets production in leptonic final states as a function of the number of jets as measured by (a) ATLAS [19] and (b) CMS [21]. Data points with full uncertainties are compared to the Born description in blue, QCD dijet production with WS in green, and the sum of the two contributions in red. Simulation uncertainties are statistical only.

the CTEQ6L1 PDF set. The Monash tune [56] is used which sets $\alpha_s = 0.1365$ within the PS. The Z mass is required to be above 40 GeV and PS emissions are allowed up to the kinematic limit of $p_T = \sqrt{s}/2$ to avoid gaps in phase space (known as “power showers”).

The Born description does not yield the correct normalisation of the cross-section and, consequently, an overall scaling is applied (the so-called “K-factor”). K-factors are chosen empirically by scaling the Born contribution to agree with the data. Centrally, the K-factor for Z +jets is taken to be 1.37 based on the zero-jet bin of the exclusive jet multiplicity distribution, N_{jet} . The K-factor for W +jets is determined to be 1.28 based on the one-jet bin of the N_{jet} distribution. In the forward region, the Born contribution is scaled by 1.10 to enforce agreement with the $[10 - 20]$ GeV bin of the Z +jet cross-section as a function of p_T^{jet} . Empirically, it is seen that a LO prediction of QCD dijet production does not need a K-factor but rather an enhancement of α_s can compensate for missing higher orders [57]. Here, $p_T^{Z/W}$ is required to be above 1 GeV with respect to the parton in the shower to remove divergences. Double counting between the Born and WS contributions are removed as described in Sect. 6 with a k_T algorithm R parameter of 0.6.

The comparisons in Figs. 11-14 demonstrate that a significant improvement in the modelling of the data is achieved with the inclusion of WS. The number of events with a high jet multiplicity is increased and a better description of p_T^{jet} is achieved. What is more, Figs. 12 and 13 demonstrate that the weak shower contribution becomes increasingly dominant for subleading jets.

The description of event shapes, while not perfect, is also improved as seen in Fig. 14. This is to be expected from a LO description.

Figs. 11 and 15 demonstrate that the high N_{jet} and high p_T^{jet} regions, respectively, is overestimated by the combined prediction. This can be attributed to the use of power showers and a value for the strong coupling, α_s^{PS} , that is significantly higher than the

best-fit NLO value at the Z mass pole, α_s^{NLO} . Together these serve to compensate for missing higher orders in the calculations. However, the former involves a stretching of the PS beyond its formal region of validity and the effect of the latter grows as $(\alpha_s^{\text{PS}}/\alpha_s^{\text{NLO}})^{N_{\text{jet}}}$. It is, therefore, not surprising that the modelling of high N_{jet} events is poor, in particular.

It is evident that LHCb does not yet probe regions of phase space where WS becomes a significant contribution as is illustrated in Figs. 16 and 17. The Born description does not fully account for the data at high $p_{\text{T}}^{\text{jet}}$ and low $\Delta\phi$, but neither does the WS component significantly improve agreement with data. Overall, a good description of the LHCb measurement is not achieved in this case.

As a side note, Fig. 16 (b) shows individual contributions to the weak shower from ranges of outgoing partonic p_{T} in the centre-of-mass frame of the underlying $2 \rightarrow 2$ process. The figure demonstrates that relatively small values of parton transverse momentum can lead to significant subleading contributions to the WS. Specifically, the $[10 - 20]$ GeV range is the third most important contribution to the first bin of $p_{\text{T}}^{\text{jet}}$. This fact is surprising given that W and Z are significantly heavier than the scale of the process and very little phase space is expected to be available for the emission of a massive gauge boson. Emissions are made possible, however, due to the interplay between the large dijet production cross-section at these values of p_{T} and the fact that PYTHIA treats the phase space of the event holistically.

Finally, Fig. 18 shows the p_{T} spectra of W daughters in leptonic decays, p_{T}^l , for the Born and weak shower description. No acceptance cuts have been applied in this case. It is clear that leptons which originate from the PS have a wider Jacobian peak and have the effect of smearing the p_{T}^l distribution and increasing the contribution from high- p_{T}^l events. This impacts EW analyses that use fits to the p_{T}^l distribution to extract physical quantities such as event yields or the W boson mass.

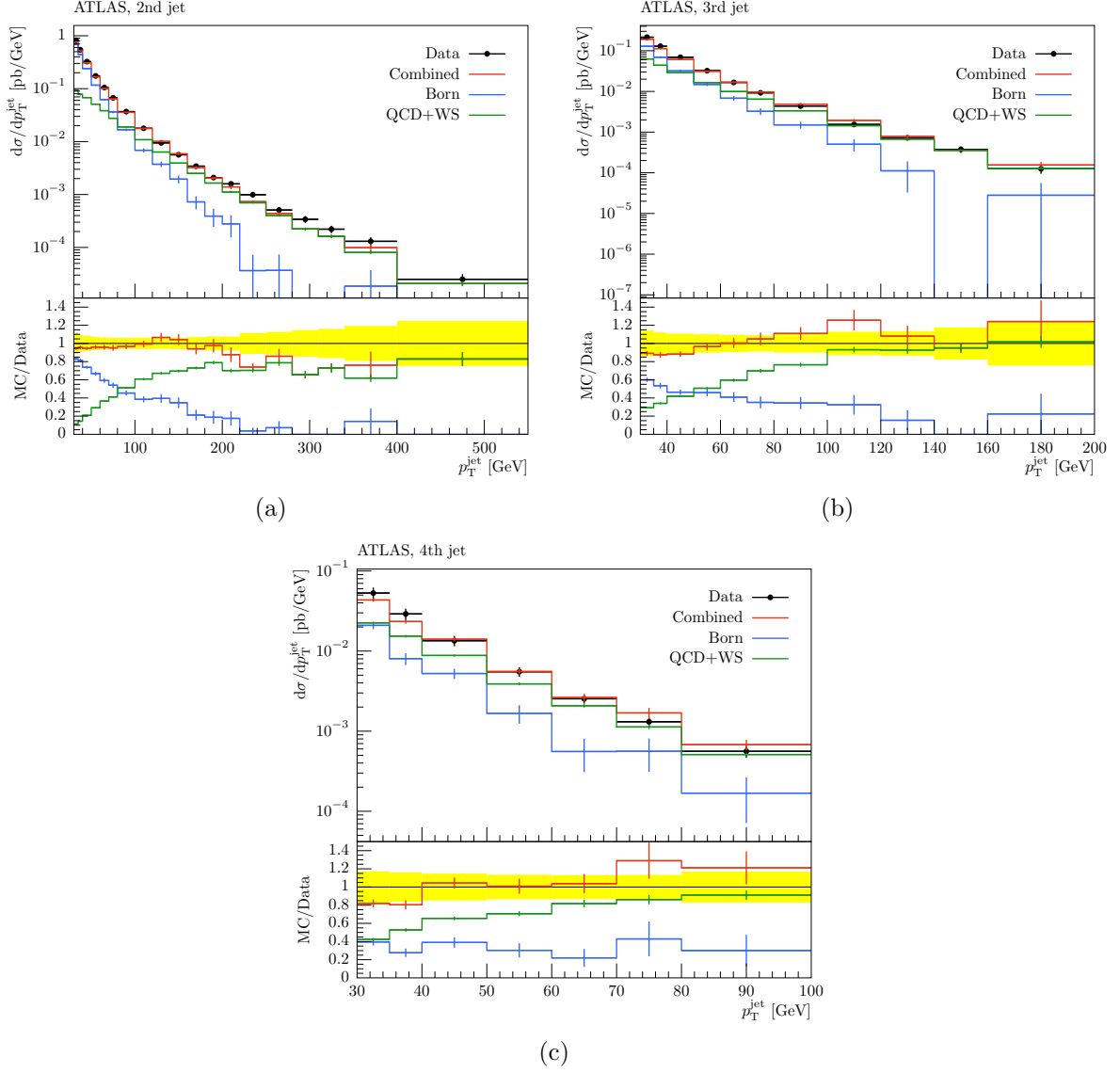


Figure 12: Differential cross-section for Z +jets production in leptonic final states as a function of p_T^{jet} for subleading jets as measured by ATLAS [19]. Data points with full uncertainties are compared to the Born description in blue, QCD dijet production with WS in green, and the sum of the two contributions in red. Simulation uncertainties are statistical only.

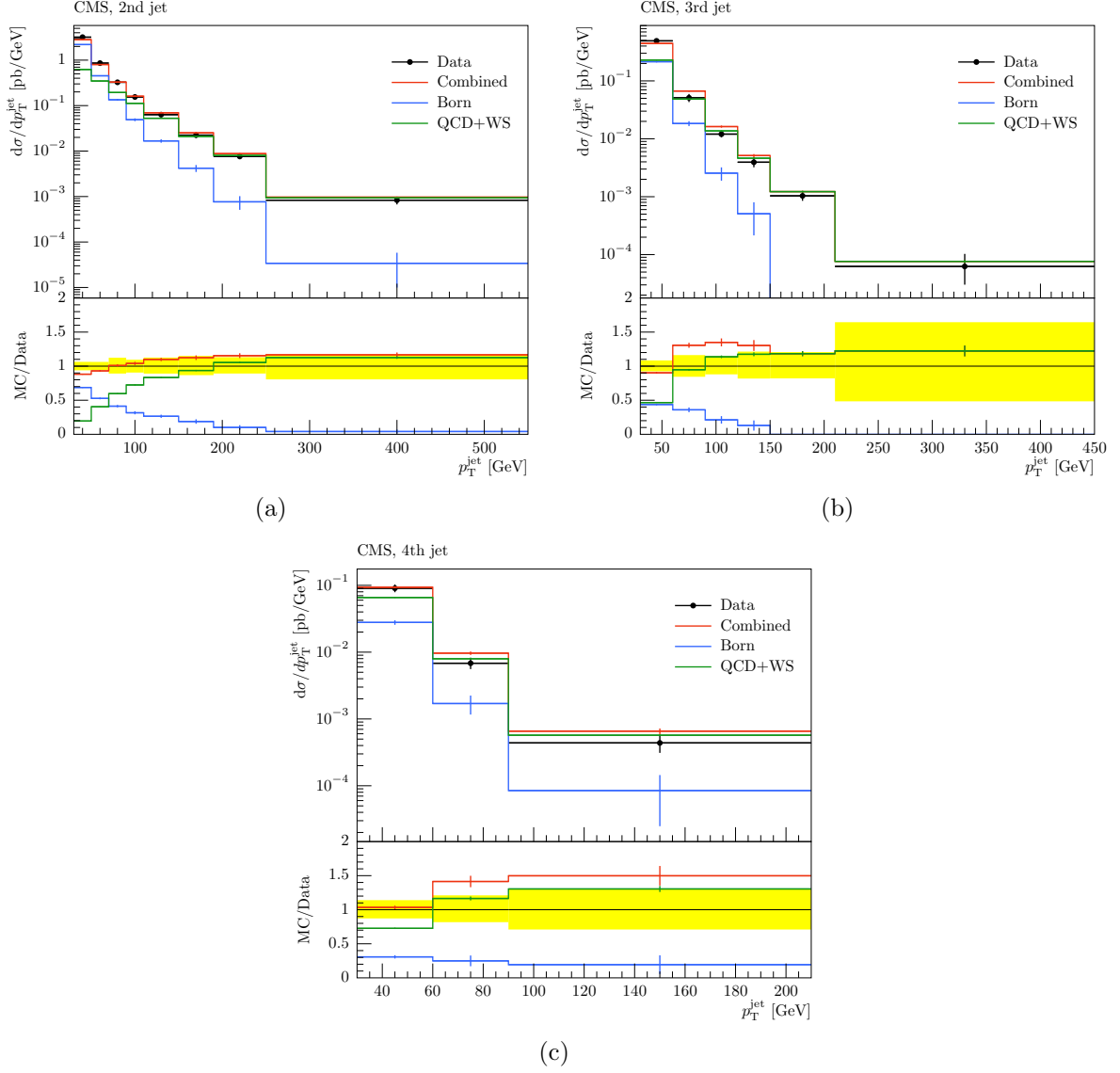


Figure 13: Differential cross-section for W +jets production in leptonic final states as a function of p_T^{jet} for subleading jets as measured by CMS [21]. Data points with full uncertainties are compared to the Born description in blue, QCD dijet production with WS in green, and the sum of the two contributions in red. Simulation uncertainties are statistical only.

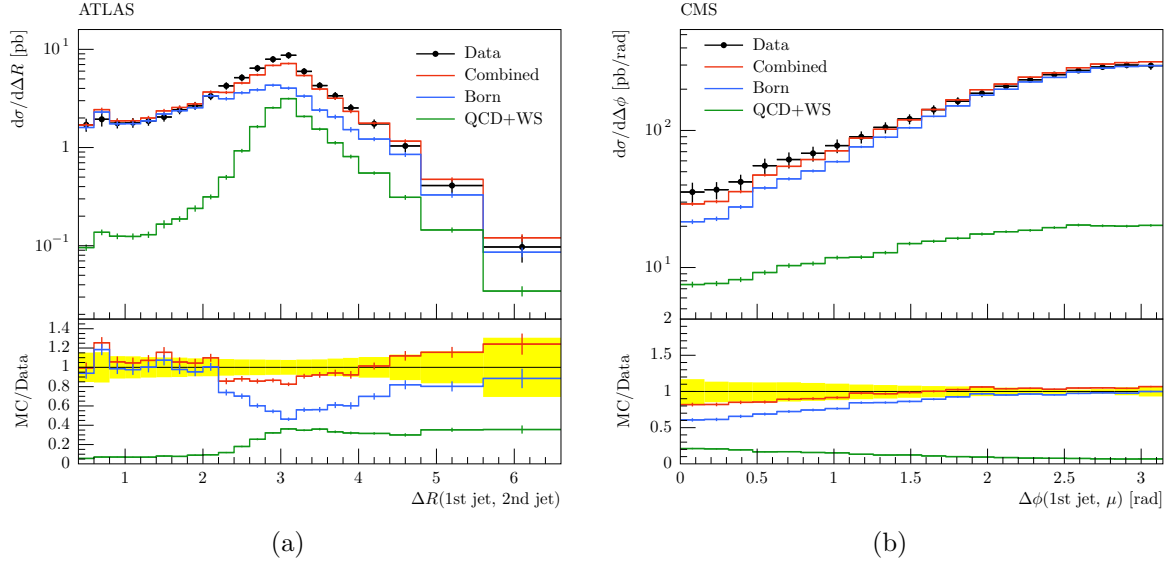


Figure 14: Differential cross-section for (a) Z +jets production as a function of the radial distance between jets as measured by ATLAS [19] and (b) W +jets production as a function of the azimuthal angle between the muon and the leading jet as measured by CMS [21]. Data points with full uncertainties are compared to the Born description in blue, QCD dijet production with WS in green, and the sum of the two contributions in red. Simulation uncertainties are statistical only.

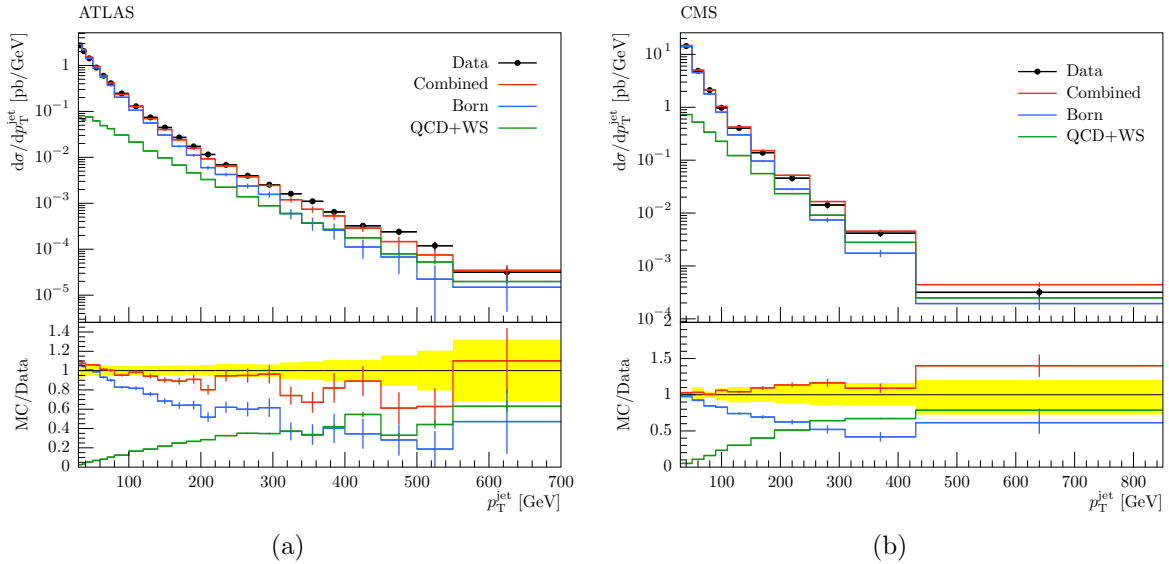


Figure 15: Differential cross-section for (a) Z +jets production and (b) W +jets production in leptonic final states as a function of the transverse momentum of the leading jet as measured by (a) ATLAS [19] and (b) CMS [21]. Data points with full uncertainties are compared to the Born description in blue, QCD dijet production with WS in green, and the sum of the two contributions in red. Simulation uncertainties are statistical only.

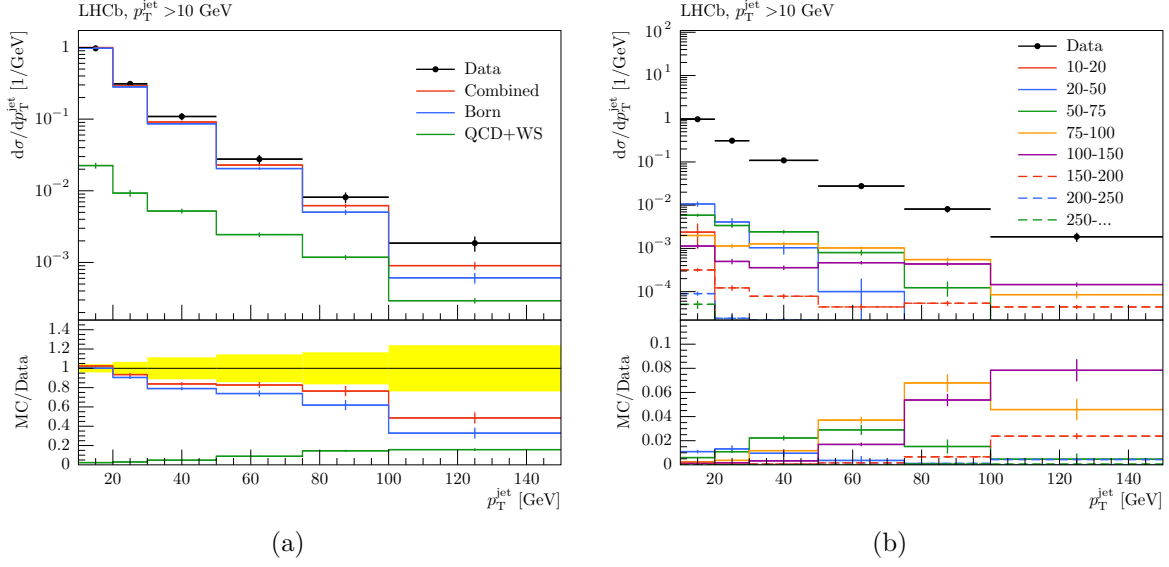


Figure 16: Differential cross-section for Z +jets production in the muon final state as a function of p_T^{jet} as measured by LHCb [22]. In (a) Data points with full uncertainties are compared to the Born description in blue, QCD dijet production with WS in green, and the sum of the two contributions in red. In (b) individual contributions from ranges of outgoing parton transverse momenta in the centre-of-mass frame in dijet production are illustrated. Simulation uncertainties are statistical only.

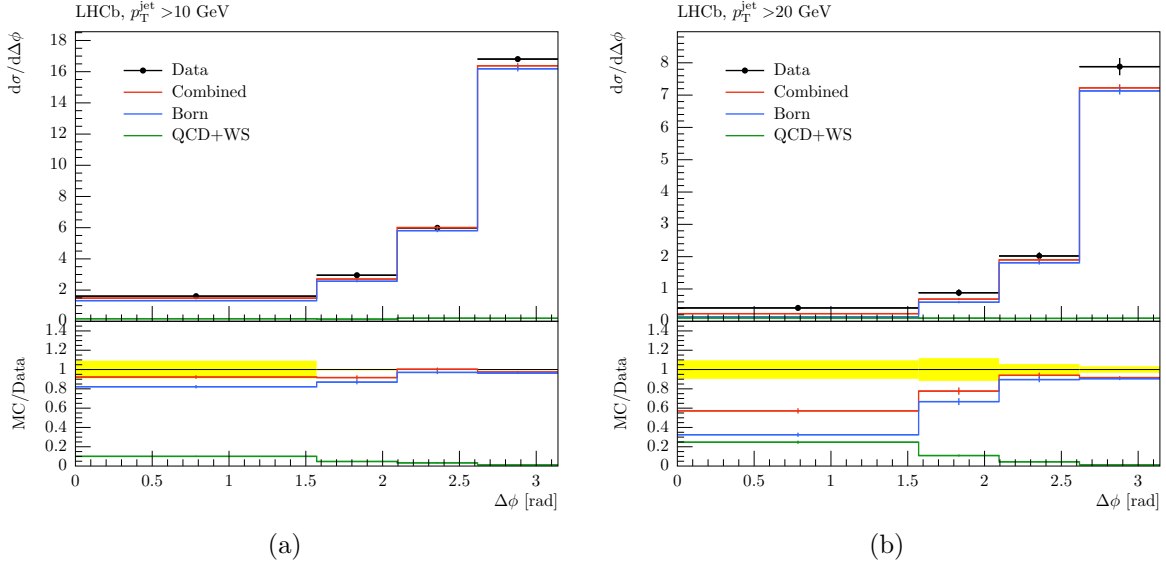


Figure 17: Differential cross-section for Z +jets production in the muon final state as a function of the azimuthal angle between the Z and the leading jet for (a) $p_T^{\text{jet}} > 10$ GeV and (b) $p_T^{\text{jet}} > 20$ GeV as measured by LHCb [22]. Data points with full uncertainties are compared to the Born description in blue, QCD dijet production with WS in green, and the sum of the two contributions in red. Simulation uncertainties are statistical only.

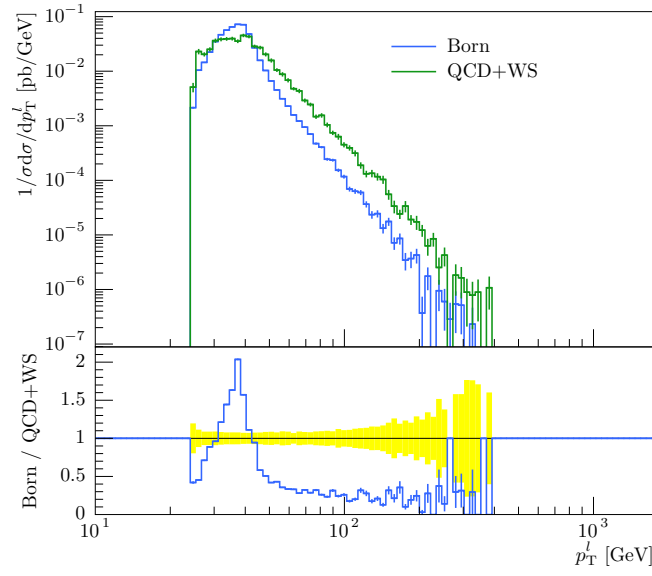


Figure 18: The lepton transverse momentum distribution in the Born description in blue is compared to QCD dijet production with WS in red. Uncertainties are statistical only and no acceptance cuts have been applied.

8 Conclusions

This note presents a study of M&M schemes and WS. These novel advanced theoretical tools are compared to measurements performed at the LHC by the ATLAS, CMS, and LHCb collaborations at $\sqrt{s} = 7$ TeV and $\sqrt{s} = 13$ TeV.

M&M schemes are seen to provide a good description of event shapes in the central and forward regions and to model p_T^{jet} and p_T^Z distributions accurately in the forward region. WS, while accurate to LO only, is able to significantly improve the description of the jet multiplicity and p_T^{jet} distributions centrally. WS also yields an improvement in the modelling of event shapes. Finally, measurements performed at LHCb do not yet access regions of phase space where WS is expected to be dominant. WS becomes a significant, or even the dominant, production mechanism of EW bosons for event topologies with two, or more, jets and scales beyond 100 GeV in p_T^{jet} . It is clear, however, that with increased data at higher centre-of-mass energies will improve the reach of measurements performed at LHCb. In parallel, WS effects such as the suppression of the jet rate as well as multiple emissions are expected to become more common at these energies.

This study constitutes a test of precise theoretical tools in a novel region of phase space. It proves that a variety of M&M schemes can be employed with some confidence in modelling EW boson production in association with jets. Finally, it is clear that with the extraordinary success of the SM and with beyond-the-Standard-Model physics proving elusive, increased precision is required in both the experimental measurements' programme at the LHC as well as in developing theoretical tools such as matching and merging and weak showering.

9 Acknowledgements

We take this opportunity to thank Leif Lönnblad and Torbjörn Sjöstrand for their expert guidance during the course of this research. We would also like to acknowledge the invaluable help we received from Jesper Roy Christiansen and Stefan Prestel and the entire Lund theory group. Finally, we would like to thank David Ward for improving the quality of this note and for many helpful suggestions. This work was supported in part by the European Union as part of the FP7 Marie Curie Initial Training Network MCnetITN (PITN-GA-2012-315877).

References

- [1] ATLAS collaboration, G. Aad *et al.*, *Measurement of the inclusive W^\pm and Z/γ^* cross sections in the electron and muon decay channels in pp collisions at $\sqrt{s} = 7$ TeV with the ATLAS detector*, Phys. Rev. **D85** (2012) 072004, [arXiv:1109.5141](#).
- [2] ATLAS collaboration, G. Aad *et al.*, *Measurement of the double-differential high-mass Drell-Yan cross section in pp collisions at $\sqrt{s} = 8$ TeV with the ATLAS detector*, JHEP **08** (2016) 009, [arXiv:1606.01736](#).
- [3] ATLAS collaboration, G. Aad *et al.*, *Measurement of W^\pm and Z -boson production cross sections in pp collisions at $\sqrt{s} = 13$ TeV with the ATLAS detector*, Phys. Lett. **B759** (2016) 601, [arXiv:1603.09222](#).
- [4] CMS collaboration, V. Khachatryan *et al.*, *Measurement of the transverse momentum spectra of weak vector bosons produced in proton-proton collisions at $\sqrt{s} = 8$ TeV*, [arXiv:1606.05864](#), submitted to JHEP.
- [5] CMS collaboration, V. Khachatryan *et al.*, *Measurement of the differential cross section and charge asymmetry for inclusive $pp \rightarrow W + X$ production at $\sqrt{s} = 8$ TeV*, Eur. Phys. J. C (2016) , [arXiv:1603.01803](#).
- [6] CMS collaboration, S. Chatrchyan *et al.*, *Measurement of inclusive W and Z boson production cross sections in pp collisions at $\sqrt{s} = 8$ TeV*, Phys. Rev. Lett. **112** (2014) 191802, [arXiv:1402.0923](#).
- [7] LHCb collaboration, R. Aaij *et al.*, *Measurement of forward $W \rightarrow e\nu$ production in pp collisions at $\sqrt{s} = 8$ TeV*, [arXiv:1608.01484](#), submitted to JHEP.
- [8] LHCb collaboration, R. Aaij *et al.*, *Measurement of the forward W boson production cross-section in pp collisions at $\sqrt{s} = 7$ TeV*, JHEP **12** (2014) 079, [arXiv:1408.4354](#).
- [9] LHCb collaboration, R. Aaij *et al.*, *Measurement of forward W and Z boson production in pp collisions at $\sqrt{s} = 8$ TeV*, JHEP **01** (2016) 155, [arXiv:1511.08039](#).
- [10] LHCb collaboration, R. Aaij *et al.*, *Measurement of the forward Z boson production cross-section in pp collisions at $\sqrt{s} = 7$ TeV*, JHEP **08** (2015) 039, [arXiv:1505.07024](#).
- [11] LHCb collaboration, R. Aaij *et al.*, *Measurement of the cross-section for $Z \rightarrow e^+e^-$ production in pp collisions at $\sqrt{s} = 7$ TeV*, JHEP **02** (2013) 106, [arXiv:1212.4620](#).
- [12] LHCb collaboration, R. Aaij *et al.*, *Measurement of forward $Z \rightarrow e^+e^-$ production in pp collisions at $\sqrt{s} = 8$ TeV*, JHEP **05** (2015) 109, [arXiv:1503.00963](#).
- [13] LHCb collaboration, R. Aaij *et al.*, *A study of the Z production cross-section in pp collisions at $\sqrt{s} = 7$ TeV using tau final states*, JHEP **01** (2013) 111, [arXiv:1210.6289](#).
- [14] LHCb collaboration, R. Aaij *et al.*, *Measurement of the forward Z boson production cross-section in pp collisions at $\sqrt{s} = 13$ TeV*, [arXiv:1607.06495](#), submitted to JHEP.

- [15] R. Gavin, Y. Li, F. Petriello, and S. Quackenbush, *FEWZ 2.0: A code for hadronic Z production at next-to-next-to-leading order*, Comput. Phys. Commun. **182** (2011) 2388, [arXiv:1011.3540](#).
- [16] Y. Li and F. Petriello, *Combining QCD and electroweak corrections to dilepton production in FEWZ*, Phys. Rev. **D86** (2012) 094034, [arXiv:1208.5967](#).
- [17] J. Butterworth *et al.*, *PDF4LHC recommendations for LHC Run II*, J. Phys. **G43** (2016) 023001, [arXiv:1510.03865](#).
- [18] S. Alioli *et al.*, *Precision studies of observables in $pp \rightarrow W \rightarrow l\nu$ and $pp \rightarrow \gamma/Z \rightarrow l^+l^-$ processes at the LHC*, [arXiv:1606.02330](#).
- [19] ATLAS collaboration, G. Aad *et al.*, *Measurement of the production cross section of jets in association with a Z boson in pp collisions at $\sqrt{s} = 7$ TeV with the ATLAS detector*, JHEP **07** (2013) 032, [arXiv:1304.7098](#).
- [20] CMS collaboration, S. Chatrchyan *et al.*, *Event shapes and azimuthal correlations in Z + jets events in pp collisions at $\sqrt{s} = 7$ TeV*, Phys. Lett. **B722** (2013) 238, [arXiv:1301.1646](#).
- [21] CMS collaboration, V. Khachatryan *et al.*, *Differential cross section measurements for the production of a W boson in association with jets in proton-proton collisions at $\sqrt{s} = 7$ TeV*, Phys. Lett. **B741** (2015) 12, [arXiv:1406.7533](#).
- [22] LHCb collaboration, R. Aaij *et al.*, *Study of forward Z + jet production in pp collisions at $\sqrt{s} = 7$ TeV*, JHEP **01** (2014) 033, [arXiv:1310.8197](#).
- [23] S. D. Drell and T.-M. Yan, *Partons and their Applications at High-Energies*, Annals Phys. **66** (1971) 578.
- [24] R. K. Ellis, W. J. Stirling, and B. R. Webber, *QCD and collider physics*, Camb. Monogr. Part. Phys. Nucl. Phys. Cosmol. **8** (1996).
- [25] R. Hamberg, W. L. van Neerven, and T. Matsuura, *A complete calculation of the order α_s^2 correction to the Drell-Yan K-factor*, Nucl. Phys. **B359** (1991) 343, [Erratum: Nucl. Phys. B644, 403 (2002)].
- [26] Y. Li, A. von Manteuffel, R. M. Schabinger, and H. X. Zhu, *N^3 LO Higgs boson and Drell-Yan production at threshold: The one-loop two-emission contribution*, Phys. Rev. **D90** (2014), no. 5 053006, [arXiv:1404.5839](#).
- [27] G. A. Ladinsky and C. P. Yuan, *The Nonperturbative regime in QCD resummation for gauge boson production at hadron colliders*, Phys. Rev. **D50** (1994) 4239, [arXiv:hep-ph/9311341](#).
- [28] C. Balazs and C. P. Yuan, *Soft gluon effects on lepton pairs at hadron colliders*, Phys. Rev. **D56** (1997) 5558, [arXiv:hep-ph/9704258](#).
- [29] F. Landry, R. Brock, P. M. Nadolsky, and C. P. Yuan, *Tevatron Run-1 Z boson data and Collins-Soper-Sterman resummation formalism*, Phys. Rev. **D67** (2003) 073016, [arXiv:hep-ph/0212159](#).

- [30] O. Mattelaer, <https://cp3.irmp.ucl.ac.be/projects/madgraph/wiki/Lund2014>.
- [31] G. Altarelli and G. Parisi, *Asymptotic Freedom in Parton Language*, Nucl. Phys. **B126** (1977) 298.
- [32] Y. L. Dokshitzer, *Calculation of the Structure Functions for Deep Inelastic Scattering and e^+e^- Annihilation by Perturbation Theory in Quantum Chromodynamics*, Sov. Phys. JETP **46** (1977) 641, [Zh. Eksp. Teor. Fiz. 73, 1216 (1977)].
- [33] V. N. Gribov and L. N. Lipatov, *Deep inelastic ep scattering in perturbation theory*, Sov. J. Nucl. Phys. **15** (1972) 438, [Yad. Fiz. 15, 781 (1972)].
- [34] L. Lönnblad and S. Prestel, *Unitarising Matrix Element + Parton Shower merging*, JHEP **1302** (2013) 094, [arXiv:1211.4827](#).
- [35] S. Catani, Y. L. Dokshitzer, M. H. Seymour, and B. R. Webber, *Longitudinally invariant K_t clustering algorithms for hadron hadron collisions*, Nucl. Phys. **B406** (1993) 187.
- [36] S. Catani, F. Krauss, R. Kuhn, and B. R. Webber, *QCD matrix elements + parton showers*, JHEP **0111** (2001) 063, [arXiv:hep-ph/0109231](#).
- [37] L. Lönnblad, *Correcting the color dipole cascade model with fixed order matrix elements*, JHEP **0205** (2002) 046, [arXiv:hep-ph/0112284](#).
- [38] N. Lavesson and L. Lönnblad, *W +jets matrix elements and the dipole cascade*, JHEP **0507** (2005) 054, [arXiv:hep-ph/0503293](#).
- [39] N. Lavesson and L. Lönnblad, *Merging parton showers and matrix elements: Back to basics*, JHEP **0804** (2008) 085, [arXiv:0712.2966](#).
- [40] L. Lönnblad and S. Prestel, *Matching Tree-Level Matrix Elements with Interleaved Showers*, JHEP **1203** (2012) 019, [arXiv:1109.4829](#).
- [41] M. L. Mangano, M. Moretti, F. Piccinini, and M. Treccani, *Matching matrix elements and shower evolution for top-quark production in hadronic collisions*, JHEP **0701** (2007) 013, [arXiv:hep-ph/0611129](#).
- [42] R. Frederix and S. Frixione, *Merging meets matching in MC@NLO*, JHEP **1212** (2012) 061, [arXiv:1209.6215](#).
- [43] L. Lönnblad and S. Prestel, *Merging Multi-leg NLO Matrix Elements with Parton Showers*, JHEP **1303** (2013) 166, [arXiv:1211.7278](#).
- [44] S. Höche, Y. Li, and S. Prestel, *Drell-Yan lepton pair production at NNLO QCD with parton showers*, Phys. Rev. **D91** (2015), no. 7 074015, [arXiv:1405.3607](#).
- [45] S. Höche, Y. Li, and S. Prestel, *Higgs-boson production through gluon fusion at NNLO QCD with parton showers*, Phys. Rev. **D90** (2014), no. 5 054011, [arXiv:1407.3773](#).
- [46] S. Frixione and B. R. Webber, *Matching NLO QCD computations and parton shower simulations*, JHEP **0206** (2002) 029, [arXiv:hep-ph/0204244](#).

- [47] T. Sjöstrand *et al.*, *An Introduction to PYTHIA 8.2*, Comput. Phys. Commun. **191** (2015) 159, [arXiv:1410.3012](#).
- [48] J. Alwall *et al.*, *The automated computation of tree-level and next-to-leading order differential cross sections, and their matching to parton shower simulations*, JHEP **1407** (2014) 079, [arXiv:1405.0301](#).
- [49] J. Alwall *et al.*, *A Standard format for Les Houches event files*, Comput. Phys. Commun. **176** (2007) 300, [arXiv:hep-ph/0609017](#).
- [50] J. Gao *et al.*, *CT10 next-to-next-to-leading order global analysis of QCD*, Phys. Rev. **D89** (2014) 033009, [arXiv:1302.6246](#).
- [51] P. M. Nadolsky *et al.*, *Implications of CTEQ global analysis for collider observables*, Phys. Rev. **D78** (2008) 013004, [arXiv:0802.0007](#).
- [52] A. Buckley *et al.*, *Rivet user manual*, Comput. Phys. Commun. **184** (2013) 2803, [arXiv:1003.0694](#).
- [53] J. R. Christiansen and T. Sjöstrand, *Weak Gauge Boson Radiation in Parton Showers*, JHEP **1404** (2014) 115, [arXiv:1401.5238](#).
- [54] T. Sjöstrand and P. Z. Skands, *Transverse-momentum-ordered showers and interleaved multiple interactions*, Eur. Phys. J. **C39** (2005) 129, [arXiv:hep-ph/0408302](#).
- [55] ATLAS and CMS collaborations, M. Negrini, *Review of physics results using jet substructure techniques in LHC Run1*, EPJ Web Conf. **90** (2015) 09001.
- [56] P. Skands, S. Carrazza, and J. Rojo, *Tuning PYTHIA 8.1: the Monash 2013 Tune*, Eur. Phys. J. **C74** (2014), no. 8 3024, [arXiv:1404.5630](#).
- [57] T. Sjöstrand, Private communication.